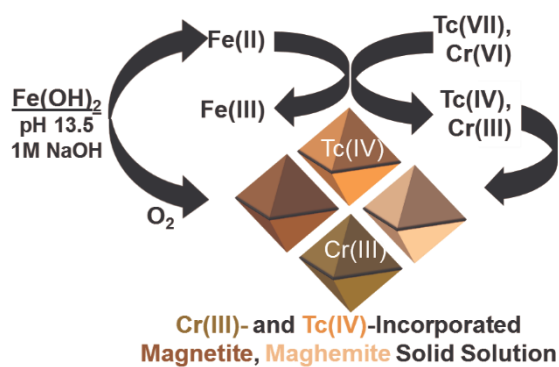


25 Tc(IV) incorporation into magnetite octahedral sites without additional substitution of Cr or Tc
26 into neighboring Fe octahedral sites. XPS analysis of Cr confirms reduction to Cr(III) and the
27 formation of a Cr-incorporated spinel, Cr_2O_3 , and $\text{Cr}(\text{OH})_3$ phases. Spinel (modeled as Fe_3O_4),
28 goethite, and feroxyhyte are detected in all samples analyzed by XRD, where Tc(IV)
29 incorporation has little effect on the spinel lattice structure. In the presence of Cr(III) a spinel
30 phase along the magnetite-chromite ($\text{Fe}_3\text{O}_4\text{-FeCr}_2\text{O}_4$) solid-solution line is formed.

31

32 TOC Graphic



34 1. Introduction

35 Nuclear waste generated from processes including fuel recycling and weapon
36 production/testing is a global concern extending beyond well-known legacy sites, e.g. Hanford
37 (Washington State, USA) and Sellafield (Cumbria, UK), creating a universal need for
38 remediation technologies that ensure long-term, safe storage of nuclear waste and contaminant
39 release prevention. One particular concern is 99-technetium (Tc), a radioactive fission product
40 especially problematic due to its long half-life (2.1×10^5 years), high fission yield (~6%), and
41 environmental mobility, as Tc(VII) species, in oxidizing subsurface environments.^{1,2} Tc
42 remediation from nuclear waste streams has numerous challenges that include: (i) reducing
43 Tc(VII) to less mobile Tc(IV) in the presence of co-mingled contaminants, especially Cr(VI),
44 that are more readily reduced than Tc(VII); and (ii) immobilizing Tc in a form that inhibits
45 reoxidation and subsequent release. Current remediation strategies target these challenges
46 separately, requiring both a reducing agent and immobilizing host material,³⁻⁵ and generates
47 excess cost and residual waste. Herein, $\text{Fe}(\text{OH})_2(\text{s})$ is investigated as a silver-bullet approach for
48 simultaneous reduction, removal, and immobilization of Tc and Cr(VI) from waste streams
49 through mineral incorporation.

50 Iron oxides and hydroxides are common industrial and environmental materials that can
51 facilitate contaminant reduction and incorporate contaminants into their crystal structure, thereby
52 shielding contaminants from re-oxidation. Cr(VI) reduction and immobilization by ferrous
53 materials has been extensively researched for a variety of environmental conditions,⁶⁻⁸ with
54 reducing agent Fe(II) present in solution^{9,10} or as a solid.¹¹⁻¹³ Similar experimental and
55 computational research efforts have investigated Tc(VII),¹⁴⁻²³ with an emphasis on Tc(IV)
56 incorporation into magnetite (Fe_3O_4). Magnetite has an inverse spinel structure,

57 $(\text{Fe}^{3+})_{\text{Tet}}(\text{Fe}^{2+}\text{Fe}^{3+})_{\text{Oct}}\text{O}_4$, where octahedral $\text{Fe(III)}_{\text{Oct}}$ substitution by metals with similar ionic
58 radii, e.g. Tc(IV) , Cr(III) , and Ti(IV) ,^{15,24,25} is a common pathway for immobilizing contaminants
59 within the mineral lattice. For example, work performed by Marshall et al.¹⁵ reports successful
60 incorporation of reduced Tc(IV) into the magnetite structure under the high pH conditions
61 expected to persist in nuclear waste streams.

62 Heretofore the simultaneous reduction, removal, and incorporation of co-mingled Tc(VII)
63 and Cr(VI) has not been studied. Building upon success immobilizing Tc(IV) in magnetite, the
64 approach described here forms magnetite via mineral transformation of $\text{Fe(OH)}_2(\text{s})$ under oxic
65 conditions via the Schikorr reaction.^{26,27} $\text{Fe(OH)}_2(\text{s})$ in solution concurrently reduces Tc(VII) and
66 Cr(VI) to Tc(IV) and Cr(III) and incorporates both contaminants into the magnetite structure. In
67 addition, the mechanism by which Tc(VII) and Cr(IV) are reduced and immobilized are
68 investigated using a suite of analytical tools to probe the oxidation state, local coordination
69 environment, and properties of the solid phases formed at the molecular-level.

70 2. Experimental

71 **$\text{Fe(OH)}_2(\text{s})$ Synthesis.** $\text{Fe(OH)}_2(\text{s})$ was prepared inside an anoxic chamber (Coy laboratories)
72 maintained with a gas mix of N_2 (98%) and H_2 (2%), an H_2/O_2 gas analyzer, and a palladium
73 catalyst for O_2 removal. $\text{Fe(OH)}_2(\text{s})$ was precipitated by dissolving 14 g of $\text{FeCl}_2 \cdot 4\text{H}_2\text{O}$ (>95%,
74 Fisher Scientific) in 400 g of double deionized water (DDI, Millipore 18 Ω) pre-purged with N_2 ,
75 adding 8.2 mL of 10M NaOH (prepared from 95% NaOH pellets, Fisher Scientific), and then
76 mixing. After reacting overnight, $\text{Fe(OH)}_2(\text{s})$ was filtered using a sterile 0.45 μm analytical filter
77 (Nalgene) and allowed to dry for 24-48 hours. Prior to experimentation, oxidized surface
78 material (if present) was removed to expose un-oxidized $\text{Fe(OH)}_2(\text{s})$ that was then reduced to a
79 powder by mortar and pestle and appropriately measured no more than 24 hours before use.

80 **Solution Preparation.** In this work a background solution of 1M NaOH (prepared from 95%
81 NaOH pellets, Fisher Scientific), was adjusted to 1560 ppm Cr(VI) with $\text{Na}_2\text{Cr}_2\text{O}_7 \cdot 2\text{H}_2\text{O}$
82 ($\geq 99.5\%$, Allied Chemical) to achieve an alkaline pH level and Cr(VI) concentration similar to
83 nuclear waste streams.²⁸ For experiments requiring Tc(VII), a 10,000 ppm NH_4TcO_4 stock
84 solution was used to adjust Cr(VI) solutions to within 1 and 1000 ppm Tc(VII). For control
85 experiments, without Cr(VI), Tc(VII) was added directly to 1M NaOH.

86 **Procedure for Tc(VII) and Cr(VI) Reduction and Removal by $\text{Fe}(\text{OH})_2(\text{s})$.** Tc(VII) and
87 Cr(VI) reduction and incorporation into iron oxides was assessed using the following procedure.
88 Approximately 0.01 to 0.5 g of $\text{Fe}(\text{OH})_2(\text{s})$ was added to solution immediately after removal
89 from the anoxic chamber. Once combined the samples were reacted for 3 days (± 1 hour) in an
90 oven set to 75°C , after which the oven was turned off and the samples allowed to cool inside the
91 oven for at least two hours. The solid material was then filtered (0.45 μm sterile analytical filter,
92 Nalgene), rinsed with ~ 50 mL of DDI, and air-dried for at least 24 hours. While filtering,
93 samples of the supernatant and DDI rinse were collected for total Cr analysis by Inductively
94 Coupled Plasma-Optical Emission Spectrometry (ICP-OES) and total Tc analysis by ICP-Mass
95 Spectrometry (ICP-MS). The final measured pH of a representative sub-set of samples was 13.5
96 ± 0.1 .

97 For select samples, the above procedure was altered to test whether sequential addition of
98 $\text{Fe}(\text{OH})_2(\text{s})$ impacted the reduction and immobilization process of Tc(VII) and Cr(VI). For these
99 samples, $\text{Fe}(\text{OH})_2(\text{s})$ was sequentially added over three days, allowing the solution to react with
100 the solid for ~ 24 hours before adding additional $\text{Fe}(\text{OH})_2(\text{s})$ or final sampling. An aliquot was
101 taken for ICP-OES and ICP-MS analysis before each subsequent addition to monitor Tc(VII) and
102 Cr(VI) removal. Additional procedure details and test matrix are provided in the supporting

103 information (SI, Section S1 and Table S1).

104 **Cr Speciation by Ion Chromatography (IC)/ICP-MS.** The details of this procedure may
105 be found in the SI. Briefly, select samples analyzed for Cr(VI) and Cr(III) in the collected
106 supernatant were separated using a chrom-FAST Chromium 3/6 Speciation Kit (CF-KIT-Cr36)
107 and SC-DX FAST auto sampler (Elemental Scientific Corporation (ESI)). ^{52}Cr was the primary
108 mass analyzed while ^{53}Cr was monitored for confirmation purposes. Cr(III) and Cr(VI) were
109 analyzed quantitatively using a Perkin Elmer ELAN DRC II quadrupole ICP-MS using time
110 resolved data points. Chromatographic peak areas were integrated using periSPEC Peak Area
111 Finder software (ESI).

112 **X-ray Photoelectron Spectroscopy (XPS).** XPS was used to evaluate the chemical
113 composition and oxidation state of Cr, Fe, and Tc at the sample near surface as a function of
114 $\text{Fe}(\text{OH})_2(\text{s})$:solution ratio and starting Tc(VII) concentration. For Tc-free samples, XPS
115 measurements were performed using a Physical Electronics Quantera Scanning X-ray
116 Microprobe equipped with a focused monochromatic Al $K\alpha$ X-ray (1486.7 eV) source for
117 excitation and a spherical section analyzer. The 80 W X-ray beam was focused to 100 μm
118 diameter and rastered over the sample. High energy resolution spectra were collected using a
119 pass-energy of 69.0 eV and 0.125 eV step size. Tc-containing samples were analyzed using a
120 Kratos Axis DLD spectrometer with a monochromatic Al $K\alpha$ X-ray (1486.7 eV) source. Spectra
121 were charge-corrected to the main line, carbon 1s peak (adventitious carbon) at 285.0 eV. Data
122 analysis and peak fitting was performed in CasaXPS (version 2.3.15). XPS peak fitting
123 procedures are detailed in the SI.

124 **X-ray Diffraction (XRD).** XRD spectra were collected using a Rigaku Miniflex II XRD unit
125 equipped with a Cu $K\alpha$ radiation ($\lambda=1.5418 \text{ \AA}$ with 30 kV and 15 mA) source. Samples

126 containing an internal standard, ~10 wt% corundum (NIST standard) or rutile (NIST or Sigma
127 Aldrich, CAS # 224227), were scanned at minimum between 3 and 90 degrees 2θ in fixed mode
128 using a 0.05 degree step size and 20 seconds/step scan speed. Mineral identification was
129 completed using Jade software (Materials Data Incorporated, California) with reference spectra
130 from the International Centre for Diffraction Data XRD database. Rietveld quantification
131 refinements were performed using Bruker TOPAS software (v5, Bruker AXS, Germany) with
132 reference patterns from published crystal structures (Inorganic Crystal Structure Database,
133 Fachinformationszentrum Karlsruhe, Germany). Mineral phase fractionation was scaled to 100%
134 by reference to the internal standard. Additional procedure details are provided in the SI.

135 **Scanning Electron Microscopy (SEM) and Energy Dispersive Spectrometry (EDS).**

136 Before SEM/EDS analysis, select samples were homogenized in a mortar and pestle, mounted on
137 an aluminum stub with double-sided carbon tape, and sputter coated with Pt (Polaron Range
138 SC7640, Quorum Technologies Ltd., East Sussex, England). SEM analysis was performed using
139 a JSM-7001F field-emission gun microscope (JEOL USA, Inc., Peabody, MA); EDS was
140 performed using a Bruker xFlash 6|60 (Bruker AXS, Inc., Madison, WI). The acceleration
141 voltage during imaging was 15 kV. For all analyses, $K\alpha$ positions were considered for the
142 calculations. The EDS spectra were collected for 20 s each at 80 k–100 k counts/s. Background
143 noise subtraction and atomic ratio estimates were performed using ESPRIT software (v1.9,
144 Bruker AXS, Inc.).

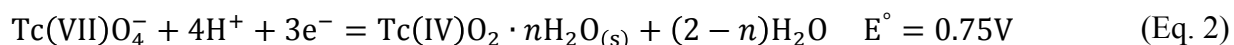
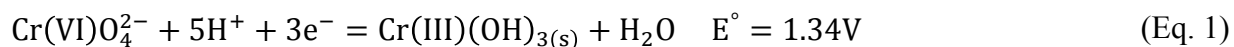
145 **X-ray Absorption Near Edge Structure (XANES) and Extended X-ray Absorption Fine 146 Structure (EXAFS) Spectroscopy.** XANES and EXAFS were used to determine the bulk 147 oxidation state and local coordination environment, respectively, of Tc once reduced and 148 immobilized within the magnetite crystal structure. Analysis was limited to samples with starting

149 Tc concentrations ≥ 11 ppm (XANES) and ≥ 100 ppm (EXAFS). Tc K edge (21044 eV) spectra
 150 were collected on beamline 11-2 at the Stanford Synchrotron Radiation Laboratory (SSRL).
 151 Dead-time correction and data reduction was performed using SixPack.²⁹ Data analysis was
 152 performed using ATHENA/ARTEMIS software.³⁰ XANES spectra were energy calibrated using
 153 TcO_4^- adsorbed on Reillex-HPQ and fit using a linear combination of Tc(IV) and Tc(VII)
 154 standards.³¹ For EXAFS fitting, a Tc-substituted magnetite structure was used in addition to
 155 models for $\text{TcO}_2 \cdot 2\text{H}_2\text{O}$ and TcO_4^- as necessary.^{14,31,32} Additional analysis details are provided in
 156 the SI.

157 3. Results and Discussion

158 **Tc(VII) and Cr(VI) Removal by $\text{Fe}(\text{OH})_2(\text{s})$.** Percent removal of Cr and/or Tc from
 159 solution was determined as a function of $\text{Fe}(\text{OH})_2(\text{s})$:solution ratio (Figure 1). In the absence of
 160 Cr(VI), 1 ppm of Tc(VII) is removed ($>99.5\%$) with a minimum $\text{Fe}(\text{OH})_2(\text{s})$:solution ratio of
 161 0.005 g/mL; however, in the presence of 1560 ppm Cr(VI), an $\text{Fe}(\text{OH})_2(\text{s})$:solution ratio of 0.02
 162 g/mL is required to completely remove Cr(VI) and Tc(VII) ($>99.7\%$). This same
 163 $\text{Fe}(\text{OH})_2(\text{s})$:solution ratio is required to remove Cr(VI) from solution in the absence of Tc(VII).

164 Assuming Cr(VI) and Tc(VII) removal is contingent on reduction to Cr(III) and Tc(IV) first,
 165 the Fe(II) required for reduction can be assessed as follows. Cr(VI) and Tc(VII) require three
 166 electrons each for reduction to Cr(III) and Tc(IV).³³



167 Provided that Cr(VI) and Tc(VII) are present in solution at a combined concentration of
 168 0.030 eq/L, only 0.09 Fe(II) eq/L is required for complete reduction to Cr(III) and Tc(IV). The
 169 experimentally determined $\text{Fe}(\text{OH})_2(\text{s})$:solution ratio needed to remove Tc(VII) and Cr(VI) from

170 solution, 0.02 g/mL, is equivalent to 0.22 Fe(II) eq/L and over double the required Fe(II)
171 equivalents needed. Excess Fe(II) is likely needed to off-set rapid oxidation of Fe(II) to Fe(III)
172 under oxic conditions and generate Fe(III) necessary to form iron oxide phases, such as
173 magnetite ($\text{Fe}^{2+}\text{Fe}_2^{3+}\text{O}_4$) and goethite ($\alpha\text{-FeOOH}$), capable of incorporating Cr(III) and Tc(IV)
174 into their mineral structure.^{12,13,15,20,21}

175 Surprisingly, when Cr(VI) and Tc(VII) are both present in solution, reduction and removal of
176 both constituents occurs concurrently, despite a more favorable reduction potential for Cr(VI)
177 versus Tc(VII), 1.34 V and 0.748 V, respectively.³³ This is most evident in Figure 1, where if
178 Cr(VI) was completely removed before Tc(VII), an increase in Tc(VII) removal would not be
179 observed with partial removal of Cr(VI) at $\text{Fe}(\text{OH})_2(\text{s})$:solution ratios between 2.5×10^{-3} and 0.01
180 g/mL.

181 **Cr(VI) Reduction by $\text{Fe}(\text{OH})_2(\text{s})$.**

182 *Speciation of Cr Remaining in the Supernatant.* From preliminary control experiments
183 focusing on the removal of Cr(VI) in the absence of Tc(VII), two duplicate samples were
184 analyzed by IC/ICP-MS to determine the speciation of Cr remaining in solution, after partial
185 removal by $\text{Fe}(\text{OH})_2(\text{s})$ ($\text{Fe}(\text{OH})_2(\text{s})$:solution ratio, 0.01 g/mL). For both samples, Cr was 85(1)%
186 removed from solution. Samples were analyzed for Cr(VI) and Cr(III) using isotopes ^{52}Cr and
187 ^{53}Cr . Table 1 reports these values and the isotopic average. The non-detect levels of Cr(III) by
188 this method confirm that Cr remaining in the supernatant is almost completely Cr(VI).

189 *Speciation of Cr in the Solid Phase.* The speciation of Cr was analyzed by XPS for select
190 solid samples. XPS high resolution narrow scans for Cr are shown in Figure 2A for three Cr-
191 containing solid samples (no Tc) for $\text{Fe}(\text{OH})_2(\text{s})$:solution ratios 0.005, 0.01, and 0.06 g/mL. Peak
192 fitting was performed only for the Cr $2p_{3/2}$ peak, due to the complexity of the Cr region. Cr(VI)

193 was fit as one peak and Cr(III) species fit separately as Cr_2O_3 , chromite (FeCr_2O_4), and $\text{Cr}(\text{OH})_3$.
194 Procedure details for peak fitting are provided in SI, section S2, and a phase distribution
195 summary is provided in Table 2. From peak fitting results, <6.91 atomic (at) % Cr(VI) is present
196 on the sample near surface (top ~10 nm), with the remainder of the Cr present as Cr(III)
197 incorporated into the spinel phase (modeled as chromite, FeCr_2O_4) or as Cr_2O_3 and $\text{Cr}(\text{OH})_3$.

198 The distribution of Cr(III) between the three modeled phases can be justified when
199 considering the Cr:Fe ratio detected on the surface (Table 2), determined from the relative XPS
200 surface composition (Table S3). At a 0.005 g/mL $\text{Fe}(\text{OH})_2(\text{s})$:solution ratio, the sample near
201 surface has a Cr:Fe ratio of 4.39 and only 9.24 at% Cr is incorporated as FeCr_2O_4 . The remaining
202 Cr(III) is mostly distributed between Cr_2O_3 and $\text{Cr}(\text{OH})_3$. However, an increase in the
203 $\text{Fe}(\text{OH})_2(\text{s})$:solution ratio, to 0.01 g/mL, lowers the surface Cr:Fe ratio to 1.52 and increases
204 Cr(III) incorporation into chromite to 47.3 at%. This chromite increase is consistent with similar
205 work⁹ and attributed to an increase in Fe(II) available to reduce Cr(VI) and incorporate Cr(III)-
206 into FeCr_2O_4 . Deviation from this trend is observed at an $\text{Fe}(\text{OH})_2(\text{s})$:solution ratio of 0.06 g/mL,
207 where nearly 97 at% Cr is associated with Cr_2O_3 and $\text{Cr}(\text{OH})_3$; however, given the extremely low
208 Cr:Fe ratio, 0.12, little Cr is present on the surface. This is likely due to the presence of excess
209 Fe(II) that forms an Fe-oxide passivation layer on the surface of Cr-containing solids. The
210 presence of a passivation layer is supported by the spinel parameter calculated from respective
211 XRD spectra, where there is an increase in magnetite-like structure with decreasing Cr:Fe ratio
212 (Table 2).

213 SEM images and EDS measurements provided in the SI (Section S4) further support an
214 increase in spinel and Cr-incorporated spinel phase formation with a decrease in the starting
215 concentration ratio of Cr:Fe. This is evident from the near micron size spinel crystals imaged at

216 lower Cr:Fe ratios and the composition determined by EDS matches that of magnetite within
217 error (43 at% Fe and 57 at% O).

218 **Tc(VII) Reduction by Fe(OH)₂(s).** A mechanism similar to that for Cr(VI) reduction and
219 incorporation is expected for Tc(VII). The oxidation state of Tc in the solid phase was
220 determined by XANES. XANES spectra were fit (Figure 3, left panel) using a linear combination
221 of TcO₄⁻ and TcO₂·2H₂O standards to determine the fraction of Tc(VII) and Tc(IV) species
222 (Table 3). As expected, an increase in the initial Fe:Tc ratio, calculated from the moles of Tc and
223 Fe(II) added at the start of the experiment (SI Section S5), correlates with an increase in
224 reduction of Tc(VII) to Tc(IV); however, some Tc(VII) is still present at the lowest Fe:Tc molar
225 ratio. This could be due to Tc(IV) reoxidation to Tc(VII), TcO₄⁻, between sample preparation and
226 analysis (~3 weeks). For all other samples analyzed by XANES, little to no Tc(VII) is present.
227 Furthermore, based on these results, Cr does not seem to hinder the reduction of Tc(VII) despite
228 redox potentials ((Eq. 1 and (Eq. 2) favoring Cr reduction.

229 For comparison, samples analyzed by XANES were also analyzed by XPS to compare bulk
230 phase results to those of the near surface. A summary of these results is provided in Table 3 and
231 detailed in SI, Section S2. Overall the presence of Tc on the sample near surface is minimal,
232 ranging from 0 to 0.81 at% with decreasing Fe:Tc ratio. Tc 3d_{5/2} and 3d_{3/2} peak fitting of high
233 resolution narrow scans (Figure 2B) show an increase in Tc(IV) on the sample surface with
234 increasing Fe:Tc, ranging from 57.64% to 84.35% for those samples where Tc was detected.
235 Since XPS is surface sensitive and XANES characterizes the bulk phase, XPS detection of
236 Tc(VII) on the surface of samples otherwise undetectable by XANES is not surprising, though
237 does not discount the efficacy of Fe(OH)₂(s) for the reduction and removal of Tc(VII) based on

238 the trends described. Some re-oxidation of Tc(IV) is expected upon exposure to air over
239 extended time periods,¹⁵ a challenge that will be targeted in future work.

240 **Local Coordination Environment of Tc(VII) by EXAFS.** Fe(OH)₂(s) suspended in
241 solution will rapidly form magnetite (Fe₃O₄) under oxidizing conditions. The formation of
242 magnetite is driven by electron transfer between Fe(II) and Fe(III) ions and dissolution
243 crystallization, depending on available Fe(II) and metal ion substitution into the crystal
244 structure.³⁴ During this transformation, Tc(IV) can easily be incorporated into the mineral
245 structure, as it has the same ionic radii as Fe(III), 0.785 Å,³⁵ thereby protecting Tc(IV) from
246 reoxidation. To evaluate Tc(IV) incorporation into magnetite in the presence of Cr(VI)/Cr(III)
247 the local coordination environment was determined for select samples by EXAFS. Figure 3
248 (middle and right panels) shows collected EXAFS spectra, their Fourier transforms, and fits. A
249 Tc-incorporated modified magnetite model³² was used to fit all samples, with some samples
250 requiring additional pathways to account for Tc(IV) precipitated on the surface, modeled by
251 TcO₂·2H₂O,³¹ and surface pertechnetate (TcO₄⁻).¹⁴ EXAFS fit parameters for samples and
252 models are outlined in Tables S7 and S8, respectively. A Tc-incorporated goethite (α-FeOOH)
253 model was also considered during early stages of analysis, but failed to accurately fit the data.
254 Partial substitution of Tc and/or Cr into the nearest neighboring Fe octahedral site (Fe1, S7) did
255 not improve any sample fits. Finally, including first shell oxygen at 2.47 Å to account for
256 hydrated oxygen in TcO₂·2H₂O did not contribute significantly to the sample fit for Fe:Tc ratio
257 491, despite the presence of Tc at ~2.57 Å. This is attributed to TcO₂·2H₂O Tc(IV) atoms being
258 partially incorporated into magnetite, convoluting signal due to TcO₂ hydration.^{15,36,37}

259 Based on the coordination numbers determined from EXAFS fits, the fractional composition
260 of each sample was determined for TcO₄⁻, TcO₂·2H₂O, and Tc-incorporated magnetite (Table 3)

261 and is graphically shown in Figure 4. The results agree with the fraction of Tc(VII) versus Tc(IV)
262 determined by XANES. From Figure 4, it is apparent that with increasing Fe:Tc there is a steady
263 increase in Tc-incorporated magnetite; however, total incorporation of Tc into magnetite is not
264 achieved at the Fe:Tc ratios analyzed. For a 56 Fe:Tc ratio, with no Cr added, Tc is largely
265 present as $\text{TcO}_2 \cdot 2\text{H}_2\text{O}$ and TcO_4^- , with only 17(5)% Tc incorporated into magnetite. The high p
266 value (0.082) associated with incorporating octahedral Fe (magnetite, Fe1) indicates that it does
267 not significantly improve the fit and supports Tc mostly present as $\text{TcO}_2 \cdot 2\text{H}_2\text{O}$ and TcO_4^- .
268 Alternatively, when 1560 ppm Cr is added, Tc-incorporated magnetite increases to 20(4)% and
269 TcO_4^- decreases from 28(2)% to 10(2)%. This suggests Tc(VII) reduction is not hindered by
270 Cr(VI) and the formation of Cr-oxide/hydroxide passivation layers (XPS Analysis, Table S2)
271 could reduce risk of Tc(IV) reoxidation and dissociation from magnetite.^{12,13} For larger Fe:Tc
272 ratios, 208 and 491, TcO_4^- is not detected, and while $\text{TcO}_2 \cdot 2\text{H}_2\text{O}$ remains the dominant Tc phase,
273 Tc-incorporated magnetite steadily increases with Fe:Tc ratio, reaching a maximum of 44(5)%.
274 This trend is consistent with previous for larger Fe:Tc ratios, where Tc-incorporated magnetite is
275 the dominant Tc phase.^{21,23}

276 **Solid Phase Characterization by XRD.** Solid mineral phase distribution as a function of
277 $\text{Fe}(\text{OH})_2(\text{s})$:solution ratio, Cr(VI) and Tc(VII) concentration was determined by XRD. Previously
278 mentioned, a decrease in the magnetite lattice a parameter, 8.396 Å, to values near 8.378 Å
279 (chromite) or 8.34 Å (maghemite, $\gamma\text{-Fe}_2\text{O}_3$) can elucidate ion substitution and mineral
280 transformation processes.^{38,39} Figure 5 provides examples of XRD patterns for samples exposed
281 to Cr(VI) and/or Tc(VII), a control sample (no Cr(VI) or Tc(VII)), and reference spectra for
282 magnetite, feroxyhyte ($\delta\text{-FeO}(\text{OH})$), and goethite. From quantification and refinement
283 calculations (Table S4), the primary phases present in all samples are goethite, feroxyhyte,

284 spinel, and amorphous (unidentified) phases. Since magnetite, chromite, and maghemite spinels
285 could not be individually resolved, quantification and refinement calculations only incorporate
286 one spinel phase, magnetite.

287 At low concentrations, 1 ppm, Tc is expected to be predominantly incorporated into the
288 magnetite structure based on the increase in Tc incorporation extrapolated from EXAFS phase
289 distributions (Figure S8). This assumption is supported by the calculated spinel *a* parameter,
290 8.3944(2) Å, which nearly matches magnetite (8.396 Å)^{38,39} and indicates negligible distortion of
291 the crystal structure upon Tc incorporation. Additionally, compared to the control sample formed
292 in the absence of Tc and Cr(VI), spinel formation increased from 27% to 48%, suggesting that
293 the presence of Tc might drive spinel formation over other phases.

294 Detailed previously, Cr(VI) addition drives the spinel *a* parameter closer to that of chromite.
295 When 1 ppm Tc is co-mingled with Cr(VI), the spinel phase formed is minimally effected by the
296 presence of Tc and maintains a chromite-like *a* parameter, 8.3785(6) Å. However, at elevated Tc
297 concentrations, ~100 ppm, a slight increase in the *a* parameter is observed (~8.386 Å),
298 suggesting that Tc-incorporation into the spinel phase is more favorable than Cr(III)
299 incorporation. This could be due to the match in ionic radius between Tc(IV) and Fe(III), where
300 the slightly smaller ionic radius for Cr(III), 0.755 Å,⁴⁰ is less favorable for incorporation.
301 However, chromite adapts a normal spinel structure, where Fe(II) occupies the tetrahedral sites
302 and Cr(III) occupies the octahedral sites. Tc can easily be incorporated into the magnetite
303 structure without disturbing the inverse spinel crystal structure, as the data supports. However,
304 formation of chromite would require topotactic rearrangement of initially-formed magnetite to
305 incorporate Cr(III) and continue chromite formation. The energy barrier to undergo this

306 rearrangement from an inverse to normal spinel structure is proposed here to be less favorable
307 than the incorporation of Tc(IV) into magnetite.

308 Further investigation into this hypothesis is required, specifically to verify that magnetite and
309 chromite are the only two phases contributing to the spinel fraction, since the presence of
310 maghemite would also decrease the spinel lattice parameter, a .^{35,41} A comparison of samples
311 prepared under identical conditions, but analyzed by XRD within 30 days of sample preparation
312 or 30 days (or more) after preparation, show a decrease in the spinel a parameter with aging. This
313 is not surprising given that in air magnetite undergoes maghematization, in which Fe(II) is
314 oxidized to Fe(III) and the migration of excess Fe(III) atoms to the surface produces a film of
315 maghemite (γ -Fe₂O₃).⁴² The effect of maghematization will be the focus of future studies.

316 **Environmental Implications.** Successful reduction and immobilization of Tc(VII) and
317 Cr(VI) by Fe(OH)₂(s) mineral transformation provides a viable approach to treating nuclear
318 waste streams containing co-mingled Tc(VII) and Cr(VI), serving as both a reductant and
319 immobilizing agent. Once incorporated into the magnetite structure Tc(IV) is less susceptible to
320 reoxidation induced by changes in the surrounding environment, providing valuable remediation
321 opportunities for waste processing and in the natural environment. For example, Tc-incorporated
322 magnetite could be introduced into the proposed vitrification waste stream at the DOE Hanford
323 site, where magnetite-stabilized Tc would be less likely to volatilize under vitrification
324 temperatures, thus increasing Tc loading in glass waste forms. While the stability of Tc-
325 incorporated magnetite under vitrification temperature conditions is the focus of ongoing work,
326 successful integration of this work, using Fe(OH)₂(s), can also be applied to remove both Tc and
327 Cr from secondary off-gas scrubber waste streams for reducing the risk of remobilization into the
328 environment.

329 **4. Acknowledgements**

330 This research was supported by the U.S. Department of Energy's (DOE) Waste Treatment and
331 Immobilization Plant Project of the Office of River Protection. PNNL is operated for the DOE by
332 Battelle Memorial Institute under Contract DE-AC05-76RL0 1830. The XANES and EXAFS
333 data collection was carried out at the SSRL, a national user facility operated by Standard
334 University on behalf of the US DOE. A portion of the solid characterization was performed using
335 EMSL and RadEMSL, a national scientific user facility sponsored by the Department of
336 Energy's Office of Biological and Environmental Research and located at Pacific Northwest
337 National Laboratory. A portion of this work (WWL) was supported by the U.S. Department of
338 Energy, Office of Science, Basic Energy Sciences, Chemical Sciences, Biosciences, and
339 Geosciences Division (CSGB), Heavy Element Chemistry Program and was performed at
340 Lawrence Berkeley National Laboratory under contract No. DE-AC02-05CH11231

341 **5. Supporting Information**

342 Additional analysis procedures and results for Fe(OH)₂(s) addition, IC/ICP-MS, XPS, XRD,
343 SEM/EDS, XANES, and EXAFS are provided in the supporting information via the Internet at
344 <http://pubs.acs.org>.

345 **6. References**

- 346 (1) Darab, J. G.; Smith, P. A. *Chemistry of materials* **1996**, *8*, 1004.
347 (2) Luksic, S. A.; Riley, B. J.; Schweiger, M.; Hrma, P. *Journal of Nuclear Materials* **2015**, *466*,
348 526.
349 (3) Lukens, W. W.; Bucher, J. J.; Shuh, D. K.; Edelstein, N. M. *Environ. Sci. Technol.* **2005**, *39*,
350 8064.
351 (4) Fredrickson, J. K.; Zachara, J. M.; Plymale, A. E.; Heald, S. M.; McKinley, J. P.; Kennedy,
352 D. W.; Liu, C.; Nachimuthu, P. *Geochimica et Cosmochimica Acta* **2009**, *73*, 2299.
353 (5) Navrotsky, A.; Mazeina, L.; Majzlan, J. *Science* **2008**, *319*, 1635.
354 (6) Buerge, I. J.; Hug, S. J. *Environmental Science & Technology* **1997**, *31*, 1426.
355 (7) Sedlak, D. L.; Chan, P. G. *Geochimica et Cosmochimica Acta* **1997**, *61*, 2185.
356 (8) Schlautman, M. A.; Han, I. *Water Research* **2001**, *35*, 1534.
357 (9) He, Y. T.; Chen; Traina, S. J. *Environmental Science & Technology* **2004**, *38*, 5535.

- 358 (10) Pettine, M.; D'Ottone, L.; Campanella, L.; Millero, F. J.; Passino, R. *Geochimica et*
359 *Cosmochimica Acta* **1998**, *62*, 1509.
- 360 (11) He, Y. T.; Traina, S. J. *Environmental Science & Technology* **2005**, *39*, 4499.
- 361 (12) Kendelewicz, T.; Liu, P.; Doyle, C. S.; Brown Jr, G. E. *Surface Science* **2000**, *469*, 144.
- 362 (13) Kendelewicz, T.; Liu, P.; Doyle, C. S.; Brown Jr, G. E.; Nelson, E. J.; Chambers, S. A.
363 *Surface Science* **1999**, *424*, 219.
- 364 (14) Pepper, S. E.; Bunker, D. J.; Bryan, N. D.; Livens, F. R.; Charnock, J. M.; Pattrick, R. A.
365 D.; Collison, D. *Journal of Colloid and Interface Science* **2003**, *268*, 408.
- 366 (15) Marshall, T. A.; Morris, K.; Law, G. T. W.; Mosselmans, J. F. W.; Bots, P.; Parry, S. A.;
367 Shaw, S. *Environmental Science & Technology* **2014**, *48*, 11853.
- 368 (16) Kobayashi, T.; Scheinost Andreas, C.; Fellhauer, D.; Gaona, X.; Altmaier, M. In
369 *Radiochimica Acta International journal for chemical aspects of nuclear science and technology*
370 **2013**; Vol. 101, p 323.
- 371 (17) Peretyazhko, T. S.; Zachara, J. M.; Kukkadapu, R. K.; Heald, S. M.; Kutnyakov, I. V.;
372 Resch, C. T.; Arey, B. W.; Wang, C. M.; Kovarik, L.; Phillips, J. L.; Moore, D. A. *Geochimica*
373 *et Cosmochimica Acta* **2012**, *92*, 48.
- 374 (18) Smith, F. N.; Um, W.; Taylor, C. D.; Kim, D.-S.; Schweiger, M. J.; Kruger, A. A.
375 *Environmental Science & Technology* **2016**, *50*, 5216.
- 376 (19) Skomurski, F. N.; Rosso, K. M.; Krupka, K. M.; McGrail, B. P. *Environmental Science &*
377 *Technology* **2010**, *44*, 5855.
- 378 (20) Smith, F. N.; Taylor, C. D.; Um, W.; Kruger, A. A. *Environmental Science & Technology*
379 **2015**, *49*, 13699.
- 380 (21) Um, W.; Chang, H.-S.; Icenhower, J. P.; Lukens, W. W.; Serne, R. J.; Qafoku, N. P.;
381 Westsik, J. H.; Buck, E. C.; Smith, S. C. *Environmental Science & Technology* **2011**, *45*, 4904.
- 382 (22) Um, W.; Chang, H.; Icenhower, J. P.; Lukens, W. W.; Jeffrey Serne, R.; Qafoku, N.;
383 Kukkadapu, R. K.; Westsik Jr, J. H. *Journal of Nuclear Materials* **2012**, *429*, 201.
- 384 (23) Lee, M.-S.; Um, W.; Wang, G.; Kruger, A. A.; Lukens, W. W.; Rousseau, R.; Glezakou, V.-
385 A. *Nat Commun* **2016**, *7*.
- 386 (24) Muller, O.; White, W. B.; Roy, R. *Journal of Inorganic and Nuclear Chemistry* **1964**, *26*,
387 2075.
- 388 (25) McCarty, K. F.; Boehme, D. R. *Journal of Solid State Chemistry* **1989**, *79*, 19.
- 389 (26) Ma, M.; Zhang, Y.; Guo, Z.; Gu, N. *Nanoscale research letters* **2013**, *8*, 1.
- 390 (27) Schikorr, G. *Zeitschrift für Elektrochemie und angewandte physikalische Chemie* **1929**, *35*,
391 65.
- 392 (28) Russell, R. L.; Westsik Jr, J.; Swanberg, D. J.; Eibling, R. E.; Cozzi, A.; Lindberg, M. J.;
393 Josephson, G. B.; Rinehart, D. E. *US Department of Energy Report PNNL* **2013**, 22352.
- 394 (29) Webb, S. M. *Physica Scripta* **2005**, *2005*, 1011.
- 395 (30) Ravel, B.; Newville, M. *Journal of Synchrotron Radiation* **2005**, *12*, 537.
- 396 (31) Lukens, W. W.; Bucher, J. J.; Edelstein, N. M.; Shuh, D. K. *Environmental Science &*
397 *Technology* **2002**, *36*, 1124.
- 398 (32) Wechsler, B. A.; Lindsley, D. H.; Prewitt, C. T. *American Mineralogist* **1984**, *69*, 754.
- 399 (33) Zachara, J. M.; Heald, S. M.; Jeon, B.-H.; Kukkadapu, R. K.; Liu, C.; McKinley, J. P.;
400 Dohnalkova, A. C.; Moore, D. A. *Geochimica et Cosmochimica Acta* **2007**, *71*, 2137.
- 401 (34) Jolivet, J.-P.; Chanéac, C.; Tronc, E. *Chemical Communications* **2004**, 481.
- 402 (35) Pearce, C. I.; Qafoku, O.; Liu, J.; Arenholz, E.; Heald, S. M.; Kukkadapu, R. K.; Gorski, C.
403 A.; Henderson, C. M. B.; Rosso, K. M. *Journal of colloid and interface science* **2012**, *387*, 24.

- 404 (36) Heald, S. M.; Krupka, K. M.; Brown, C. F. In *Radiochimica Acta International journal for*
405 *chemical aspects of nuclear science and technology* 2012; Vol. 100, p 243.
- 406 (37) Heald, S. M.; Zachara, J. M.; Jeon, B.-H.; McKinley, J. P.; Kukkadapu, R.; Moore, D. *X-*
407 *Ray Absorption Fine Structure--XAFS 13* **2007**, 882, 173.
- 408 (38) Deer, W. A.; Howie, R. A.; Zussman, J. *An introduction to the rock-forming minerals*; 3 ed.;
409 The Mineralogical Society: London, UK, 2013.
- 410 (39) Gorski, C. A.; Scherer, M. M. *American Mineralogist* **2010**, 95, 1017.
- 411 (40) Shannon, R. *Acta Crystallographica Section A* **1976**, 32, 751.
- 412 (41) Pearce, C. I. 2010.
- 413 (42) Sidhu, P. S.; Gilkes, R. J.; Posner, A. M. *Journal of Inorganic and Nuclear Chemistry* **1977**,
414 39, 1953.
- 415

416 **Table 1.** Cr Oxidation State in Supernatant Determined by IC/ICP-MS

Sample ^a	Total Cr	Cr(VI)	Cr(III)
	<i>ppm</i>	<i>ppm</i>	<i>ppm</i>
⁵² Cr			
Fe-DI-0.4-Cr-1	278	278	ND
Fe-DI-0.4-Cr-2	231	231	ND
⁵³ Cr			
Fe-DI-0.4-Cr-1	274	272	ND
Fe-DI-0.4-Cr-2	230	228	ND
Average ^b			
Fe-DI-0.4-Cr-1	276(3)	275(4)	ND
Fe-DI-0.4-Cr-2	230(1)	230(2)	ND

ND: Non-detect, below the detection limit.

^a Sample conditions: 1560 ppm Cr(VI), Fe(OH)₂:solution ratio = 0.01 g/mL, no Tc.

^b Average values and standard deviation in parentheses determined from ⁵²Cr and ⁵³Cr data from each replicate sample.

417

418 **Table 2.** Solid Characterization Results for Cr-Containing Solids

Fe(OH) ₂ :Solution Ratio	Cr:Fe Ratio ^a	Cr Peak Fitting				Spinel a parameter ^b
		FeCr ₂ O ₄	Cr ₂ O ₃	Cr(OH) ₃	Cr(VI)	
g/mL		<i>At%</i>	<i>At%</i>	<i>At%</i>	<i>At%</i>	<i>Å</i>
0.005	4.39	9.24	52.92	37.41	0.42	-
0.01	1.52	47.30	9.24	36.55	6.91	8.379(1) ^c
0.06	0.12	3.02	55.52	41.47	0	8.389(2)

^a Cr:Fe ratio determined from the composition at% analysis for Fe, Cr, O, and C performed using the CasaXPS software.

^b Spinel a parameter determined from XRD spectra using a magnetite reference to fit the spinel phase. Reference a parameters: magnetite = 8.396 Å, chromite = 8.379 Å, and maghemite = 8.34 Å.^{38,39}

^c Sample analyzed by XRD more than 30 days after sample preparation. Replicate sample, analyzed by XRD within 30 days of preparation, determined to have an a value = 8.3865(5) Å.

419

420